Asphaltene Precipitation in Crude Oils: Theory and Experiments

Eduardo Buenrostro-Gonzalez and Carlos Lira-Galeana
Thermodynamics Research Laboratory, Mexican Institute of Petroleum, Mexico City 07730, Mexico

Alejandro Gil-Villegas
Institute of Physics, University of Guanajuato, Leon, Guanajuato 37150, Mexico

Jianzhong Wu
Dept. of Chemical Engineering, Bourns College of Engineering, University of California, Riverside, CA 92521

DOI 10.1002/aic.10243
Published online in Wiley InterScience (www.interscience.wiley.com).

The precipitation of asphaltenes in two Mexican crude oils was measured using a combination of high-pressure isothermal expansion and atmospheric titration with n-alkanes. Experiments were carried out from the live- and tank-oil type of samples of the same crude oils. For the oils investigated, compositional data, precipitation phase diagrams, and bubble point pressures are reported. A theoretical study for these systems was performed using the statistical association fluid theory for potentials of variable range (SAFT-VR) equation of state (EOS) in the framework of the McMillan–Mayer theory. By matching a single titration curve or two precipitation onset points with this EOS, a good prediction of asphaltene precipitation over wide temperature, pressure, and composition intervals is obtained. © 2004 American Institute of Chemical Engineers *AIChE J,* 50: 2552–2570, 2004
Keywords: thermodynamic model, liquid–liquid equilibria, asphaltene precipitation, SAFT-VR EOS

Introduction

The formation and deposition of asphaltene-rich, solidlike material during oil recovery operations have been well documented in the literature (Islam, 1994; Leontaritis and Mansoori, 1988; Tutle, 1983). Field conditions conducive to precipitation include normal pressure depletion, acid stimulation, gas-lift operations, and miscible flooding, just to mention a few. The growing market of the production of crude oil in deep-water environments and the operations of enhanced oil recovery by miscible displacement are particularly sensitive to the complex phase behavior of crude oil, given that the costs of remediation and lost production resulting from organic deposition in these operations increases almost exponentially. Hence, any effort for a better understanding of the precipitation phenomena and a forecast of any possible problems is very pertinent.

The precipitation of asphaltenes is a complex phenomenon that involves asphaltenes and resins. *Asphaltenes* are defined as the fraction separated from crude oil or petroleum products upon addition of hydrocarbon solvents such as *n*-heptane (Speight, 1999). *Resins* are defined as the fraction of the desasphalted oil that is strongly adsorbed in surface-active materials such as Fuller's earth, alumina, or silica, and can only be desorbed by a solvent such as pyridine or a mixture of toluene and methanol. Asphaltenes and resins are aromatic heterocompounds with aliphatic substitutions and they form the most polar fraction of crude oil. Resins have a strong tendency to associate with asphaltenes. Such association determines, to a

Correspondence concerning this article should be addressed to C. Lira-Galeana at clira@imp.mx.

large extent, their solubility in crude oil (Koots and Speight, 1975).

According to the field experience (De Boer et al., 1995; Kokal and Sayegh, 1995) and experimental observations (Andersen, 1994; Fotland et al., 1997; Hammami et al., 2000; Thomas et al., 1992) asphaltene stability depends on a number of factors, including the composition of the surrounding fluid, pressure, and temperature. The effect of composition and pressure on asphaltene precipitation is generally believed to be stronger than the effect of temperature. Addition of paraffinic compounds shifts the solubility of asphaltenes in the bulk oil because its solvent power affects interactions among asphaltenes and resins. If the paraffinic compounds are good solvents for resins but not for asphaltenes, as the volume of diluent increases both the interaction between resins and asphaltenes and the capacity of the former to stabilize the asphaltene molecules as small aggregates becomes weak, causing asphaltenes to precipitate. Pressure depletion alone can destabilize asphaltenes and is likely the major reason for asphaltene deposition in well-bore pipes. As the density of the crude oil decreases (because of depressurization), the screening effect on asphaltene interactions arising from the presence of oil components decreases, causing the interactions between asphaltenes to become stronger, which in turn induces the precipitation.

The formation of an asphaltene phase during natural production process depends on pressure and temperature. This behavior can be represented in a *P–T* diagram, where the onset points of asphaltene precipitation are localized, drawing asphaltene stability boundaries, similarly to the conventional hydrocarbon *P–T* phase diagram (Leontaritis, 1996). This *P–T* diagram of asphaltenic fluids has been called the asphaltene precipitation envelope (APE). Published APEs are very scarce. To our knowledge, the earliest experimental study on the effect of pressure in asphaltene precipitation was made by Bilheimer et al. (1949), in mixtures of bitumen with tetralin and *n*-pentane as precipitant. They noted a consistent decrease in asphaltene precipitation as pressure increased. This observation was further validated by Lhioreau et al. (1967) in mixtures of crude oil and hydrocarbons from methane to *n*-heptane. Later APEs were published by Leontaritis and Mansoori (1988) for the Prinos oil, and by Leontaritis (1996) for South American and North American live oils. For these oils, it was observed that, as the temperature increases, the onset pressure decreases, requiring a bigger pressure change from the original reservoir *P–T* condition to initiate asphaltene precipitation. This is in agreement with other observations (Andersen, 1994; Hirschberg et al., 1984), where asphaltene solubility increased with temperature. Hirschberg et al. (1984) presented an experimental study on temperature and pressure effects on the amount and nature of asphaltenic material precipitated. According to their results, high temperatures and pressures favored asphaltene solubility and further supported evidence on the reversibility of asphaltene precipitation. Hammami et al. (2000) measured the APE for various Gulf of Mexico live oils through a series of isothermal pressure depletion experiments, obtaining evidence of asphaltene precipitation above the saturation pressure and asphaltene redissolution below this pressure, and showing that the pressure-depletion–induced asphaltene precipitation is a reversible process. The reversibility of asphaltene precipitation has been subject to question by some authors; slow kinetics of dispersion or flocculation makes it difficult to determine whether such a process is reversible (Buckley, 1999). For instance, Fotland (1997) suggested that asphaltene precipitation is an irreversible process, especially when the crude oil is under conditions far from precipitation onset. On the other hand, Joshi et al. (2001) found that asphaltene precipitation in live oils is clearly reversible with pressure, although a subtle irreversibility may occur.

Shields (2000) reported an APE measured for a Mexican crude oil. The effect of asphaltene precipitation inhibitors on the onset pressure as a function of temperature was studied by Aquino-Olivos et al. (2001) by comparing the APEs measured from live-oil fluids with different concentrations of inhibitor. Later, Aquino-Olivos et al. (2003) separated asphaltenic material from pressure-preserved bottom-hole oil samples at conditions between the onset and bubble point pressures using a bulk high-pressure filtration technique. After characterizing the separated material, important chemical and structural differences were found between this type of asphaltene and the conventional *n*-heptane asphaltenes separated by the standard procedure from expanded samples of the *same* oils.

The study of asphaltene precipitation upon addition of *n*-alkane solvents to stock-tank oils has often been used in the understanding of the precipitation phenomena. Hirschberg et al. (1984) and Chung et al. (1991) reported a series of titration experiments in tank-oil samples with liquid alkanes from *n*-pentane to *n*-hexadecane as diluents, to determine the precipitation onset composition, the amount of material precipitated, and the solubility properties of asphaltenes. Kokal et al. (1992) reported the amount of asphaltenes precipitated when two Canadian heavy oils with a high content of asphaltenes (13 and 21 wt %) were titrated with various *n*-alkanes (*n*-pentane to *n*-decane) at different dilution ratios. They observed that above a ratio of 10 mL solvent/g oil, the precipitation is completed and also a decrease in the amount precipitated at very high dilution ratios was observed, which can be attributed, in part, to a partial redissolution of asphaltenes in the solvent. Rassamdana and Sahimi (1996) measured the amount of precipitated asphaltene from an Iranian crude oil using normal alkanes with carbon number ranging from 5 to 10 at 25°C and atmospheric pressure. These authors also studied the effect of pressure and temperature on precipitation. Their results are consistent with previous observations (Hirschberg et al., 1984). A common feature in all these investigations is that the amount of precipitated material decreases as the *n*-alkane carbon number of the solvent increases, and that complete precipitation is obtained above a certain solvent/oil ratio (typically between 10 and 30 cm^3/g).

The experimental study of the effects of pressure, temperature, and composition on asphaltene precipitation has been important to understand the basic mechanisms of asphaltene phase formation, and provides the necessary input for development and validation of thermodynamic models of asphaltene precipitation, as it will be discussed next.

Modeling asphaltene precipitation

The development of asphaltene precipitation models has been based mainly on two different conceptual descriptions of asphaltene solutions: (1) asphaltenes and resins are considered as molecular entities dissolved in crude oil; and (2) asphaltene

Table 1. Properties of Dead Oil Samples, Asphaltenes, and Resins

	Mw (kg/kmol)	d (kg/m^3)	σ_A (nm)	Asphaltenes (wt %)	Resins (wt %)	Aromatics (wt %)	Saturates (wt %)
Oil C1	238.1	0.857		3.8	12.66	28.89	54.67
Oil Y3	220.2	0.861		3.25	10.88	30.73	55.14
Asphaltene (C1 and Y3)	3066	1.120	1.7				
Resins (C1 and Y3)	800	0.900	0.5				

and resin molecules form asphaltene–asphaltene and asphaltene–resin aggregates dispersed in an oil matrix.

The models corresponding to description (1) can be classified in three different categories. The first category uses the molecular solubility approach (Burke et al., 1990; Hirschberg et al., 1984; Kawanaka et al., 1991; Mannistu et al., 1997) to describe an asphaltene-containing fluid as a mixture of asphaltenes and solvent in a true liquid state, whose thermodynamic properties can be calculated from a Flory–Huggins-type solution theory, using an energy interaction parameter estimated from Hildebrand's solubility parameter. The second category corresponds to models based on cubic equations of state (EOS) (Godbole and Thele, 1992; James and Mehrotra, 1988; Kohse et al., 2000). The Godbole et al. (1992) and Kohse et al. (2000) models assume an asphaltene-containing crude oil as a multicomponent mixture, where the heaviest component is split into two components: a nonprecipitating component related to resin/asphaltene micelles that remain in the oil, and a precipitating component related to asphaltenes and resin/asphaltene micelles that form the asphaltenic phase. The third category can be represented by the model developed by Ting et al. (2003), where asphaltenes are treated as molecules whose size and nonpolar van der Waals interactions dominate the asphaltene phase behavior. The thermodynamic properties are calculated from a modified version of statistical association fluid theory (SAFT) EOS developed by Chapman et al. (1989, 1990).

Examples of the models based on description (2) are a thermodynamic–colloidal model (Leontaritis and Mansoori, 1987), a reversible micellization model (Pan and Firoozabadi, 1997; Victorov and Firoozabadi, 1996), and the McMillan–Mayer–SAFT model developed by Wu et al. (1998, 2000). The basic assumption in these models is that a crude oil can be represented by three components: asphaltenes, resins, and the solvent. In the thermodynamic–colloidal model, asphaltene precipitation is modeled by solving for the equilibrium between the resins absorbed in asphaltenes and the resins that are present in the solvent. The micellization models apply the micellization theory proposed by Nagarajan and Ruckenstein (1991). Finally, in the McMillan–Mayer–SAFT model, the McMillan–Mayer theory (Prausnitz et al., 2000) is used to model asphaltenes and resins as solutes in a continuous medium without structure.

SAFT EOS

The SAFT EOS has proved to be a very powerful approach in the prediction of the phase behavior of a wide range of systems (see Müller and Gubbins, 2001). In the SAFT-HS version of this theory, chain molecules are modeled as chains formed by tangent hard spheres interacting by van der Waals forces and associating sites, and the thermodynamic properties are described by a perturbation theory at the level of an augmented van der Waals mean-field theory. Recently, Wu et al. (1998, 2000) used the SAFT-HS approach in a molecular–thermodynamic framework based on colloid theory to describe asphaltene precipitation. Meanwhile, more robust versions of SAFT have been developed in several ways by different authors, to incorporate different theoretical descriptions of the several intermolecular forces involved in real substances. In particular, the SAFT EOS for potentials of variable range (SAFT-VR) (Galindo et al., 1998; Gill-Villegas et al., 1997) provides a more rigorous description of the thermodynamic and structural properties of the systems, using well-known results from perturbation theory for simple fluids. Intermolecular interactions can be modeled by different type of potentials, such as square-well (Galindo et al., 1998; Gill-Villegas et al., 1997) and Yukawa (Davies et al., 1999; Gill-Villegas et al., 1997). These interactions are variable-ranged potentials, and the SAFT-VR approach exploits the use of this molecular parameter to model real effects in fluids. Because in colloidal systems the screening of interactions plays a very important role, the use of a variable-ranged model is desirable to account for these effects.

This work

In this work, the effects of composition and pressure on asphaltene precipitation in two Mexican crude oils were studied experimentally. A series of titration experiments were carried out to determine asphaltene precipitation amounts in tank-oil samples with several *n*-alkanes. Also, separate high-pressure/high-temperature flocculation experiments were carried out using bottom-hole samples of the *same* oils, which enabled us to obtain the experimental APEs of these fluids. Both sets of data were modeled with a single version of the SAFT-VR EOS in the McMillan–Mayer framework developed by Wu et al. (2000). By matching a single titration curve *or* two precipitation onset points with this EOS, a good prediction of asphaltene precipitation in both low- and high-pressure conditions is obtained.

Experimental

Asphaltene precipitation by composition changes

Dead-oil samples taken from surface equipment of two problematic Mexican oil wells labeled as C1 and Y3, which are situated in the same producing region, were selected for the titration experiments with *n*-alkanes. These oils and their asphaltene/resin fractions were separated and characterized in a previous work (Buenrostro-Gonzalez et al., 2001a). Table 1 shows their general properties. The molecular weight (Mw_R) and density (d_R) of resins were taken from literature values (Peramanu et al., 1999; Speight, 1999). The asphaltene density (d_A) was measured using the method proposed by Yarranton et

Table 2. Properties of *n*-Alkanes Used as Precipitants

	Mw (kg/kmol)	*d* (kg/m^3)	Dielectric Constant	Refractive Index
n-Pentane (nC_5)	72	626.0	1.873	1.357
n-Heptane (nC_7)	100	638.0	1.921	1.388
n-Nonane (nC_9)	128	717.0	1.972	1.405
n-Dodecane (nC_{12})	170	748.0	2.012	1.422

al. (1996), and the asphaltene molecular weight (Mw_A) was determined by gel-permeation chromatography, as described elsewhere (Buenrostro-Gonzalez et al., 2001a).

Experiments were performed to determine the amounts of asphaltenes precipitated when a sample of each oil was titrated with four *n*-alkanes (nC_5, nC_7, nC_9, and nC_{12}); their properties are given in Table 2. The dead-oil samples were previously filtrated using a 0.45-μm Teflon membrane to remove any suspended material. The titration experiments (shown schematically in Figure 1), are similar to those implemented by Kokal et al. (1992) and consisted in adding a volume of *n*-alkane, corresponding to a specific titrant–oil ratio, to 5 g of dead oil in an appropriate flask. After 10 min of ultrasonic shaking, the mixture was left overnight. The solution of *n*-alkane and deasphalted oil was filtered using a vacuum system with a 0.45-μm filtration Teflon membrane (previously weighed). The flask and the filtration membrane were rinsed with small volumes of the corresponding *n*-alkane to eliminate the residual oil. The membrane with the precipitated material was dried in a vacuum oven at 0.1 bar (gauge pressure) and 333 K over 6 h and finally weighed to determine the asphaltene mass precipitated.

Asphaltene precipitation by pressure changes

Four temperature points of the upper boundary of the *P–T* APE and the corresponding bubble point pressures were measured for the live-oil samples of crude oils C1 and Y3. These samples were taken directly from the bottom of the well and were preserved by maintaining their sampling pressure until the moment of being used in the experiments. Table 3 contains the composition of the live-oil samples as measured by high-temperature gas chromatography (HTGC) and a standard characterization procedure. The C_{7+} fraction of the these samples was divided into a set of six pseudo-components, based on known average molecular weight, average density of this fraction (see Table 3), and an assumed variance. The critical properties of the six pseudo-components were estimated from their ambient-condition density and molecular weight, using Twu's correlations (Twu, 1984). Acentric factors were estimated from the Lee–Kesler correlation (Reid et al., 1984). The resulting characterizations are shown in Table 4.

Table 3. Characterization Data of Live-Oil Samples

	C1	Y3
Reservoir temperature, K	393	410
Reservoir pressure, bar	552	427
Component	mol %	mol %
CO_2	1.57	1.59
H_2S	5.39	1.44
N_2	0.91	0.47
C_1	24.02	32.22
C_2	10.09	12.42
C_3	9.58	10.29
i-C_4	1.83	2.03
n-C_4	4.83	4.87
i-C_5	2.27	2.22
n-C_5	2.74	2.71
C_6	4.77	4.12
C_{7+}		
ps-1	0.32	0.34
ps-2	6.29	5.84
ps-3	17.66	14.51
ps-4	10.99	8.06
ps-5	1.47	0.96
ps-6	0.02	0.01
Mw C_{7+}	334.66	284.36
Density C_{7+}, kg/m^3	882.2	804.8
bar = 1×10^5 Pa		

For the measurement of the APE points and the bubble points at the corresponding temperatures, a high-pressure JEFRI PVT visual cell was used. The cell is equipped with a near-infrared laser transmittance device, a solids detection system (SDS), which consists of a neon laser source of 1 μW and fiber-optic light-transmission probes (source and detector). By measuring the light transmission through the sample, this system is used to follow the changes in the opacity of the fluid, which result from density changes or formation of suspended aggregates. The PVT cell with the SDS is shown in Figure 2.

Similar to procedures described in Lira-Galeana and Hammami (2000) and Hammami et al. (2000), the oil samples were maintained at a pressure above the reservoir value during storage in high-pressure cylinders, and the cell was cleaned,

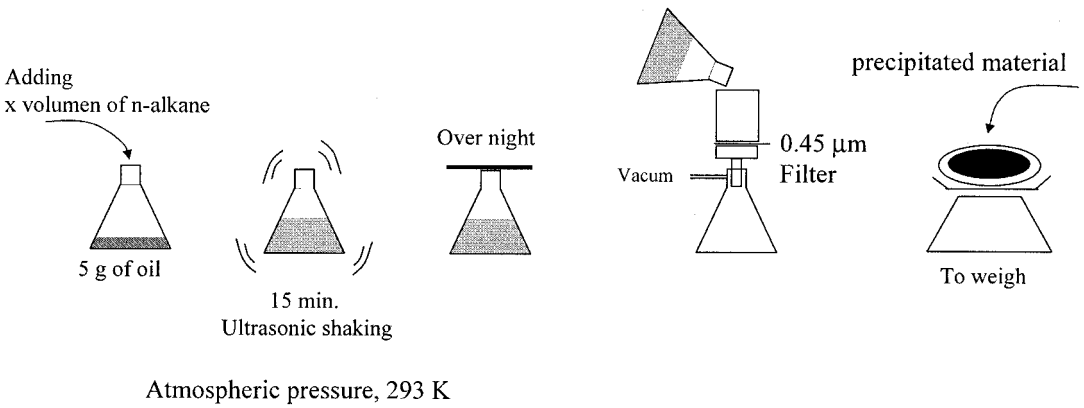

Figure 1. Crude oil titration experiment.

Table 4. Characterization of Pseudo-Components (ps-) of Live-Oil Samples

	Mw	T_b (K)	T_c (K)	P_c (bar)	ω	Z_c	Vc (m^3/kmol)	d (kg/m^3)
C1								
ps-1	264.19	611.17	779.51	13.20	0.7777	0.2207	1.08343	829.7
ps-2	296.23	647.51	814.78	12.28	0.849	0.2152	1.18772	853.6
ps-3	327.71	680.81	846.68	11.55	0.9195	0.21	1.2798	874.4
ps-4	361.09	713.18	877.52	10.95	0.9915	0.2048	1.3648	893.9
ps-5	398.57	746.59	909.17	10.40	1.0688	0.1993	1.44872	913.3
ps-6	444.68	783.60	944.14	9.86	1.1563	0.193	1.53711	934.1
Y3								
ps-1	217.96	550.66	706.1	14.12	0.7786	0.2216	0.92125	745.2
ps-2	248.83	584.43	739.74	12.66	0.8165	0.217	1.05406	772.3
ps-3	280.01	617.27	771.83	11.55	0.8637	0.2123	1.17914	797.1
ps-4	313.8	651.14	804.46	10.65	0.9217	0.2072	1.30141	821.1
ps-5	352.5	687.6	839.23	9.87	0.993	0.2015	1.42384	845.6
ps-6	352.5	687.6	839.23	9.87	0.993	0.2015	1.42384	845.6

bar = 1×10^5 Pa

evacuated, and preheated to the initial temperature before charging the samples. For each case, 30 cm^3 of live oil were transferred to the cell using a positive-displacement pump, in an isothermal step-by-step mode through the valves of the system (Figure 2) to avoid pressure changes $>$ 1 bar in the sample during the transference. The sample confined in the cell was equilibrated at the reservoir pressure and chosen temperature for 15 h before isothermal expansion. A sample of known volume was withdrawn isobarically and isothermally into an evacuated and preweighed pycnometer for gravimetric density measurement. The pressure in the cell was then decreased slowly and isothermally, by maintaining a constant negative (backward direction) pump displacement rate of 0.02 cm^3/min, while the power of transmitted light (PTL) and volume displaced are automatically measured and recorded. The cell content is mixed continuously by a magnetically coupled impeller. The expansion continues until gas begins to emit from the solution. At that point, the presence of a dispersed solid phase can no longer be resolved because the gas bubbles completely scatter the incident light and the PTL is essentially zero. If the pressure decrease continues far from the bubble point, the gas volume increases while the liquid shrinks, and eventually the volume of liquid becomes too small and the gas bubbles are sufficiently large to allow the laser beam to more easily cross the liquid–gas system that is under a strong mixing, again increasing the PTL.

The PTL refers to the amount of light that passes through the sample and is received in the detector. The PTL is inversely proportional to the density of the sampled fluid, particle size, and number of particles per unit volume of fluid. This means that, if the pressure decreases, then the PTL increases; however, if during the expansion process the size and the number of asphaltene aggregates start to increase, the opacity of the fluid also increases, decreasing the increment of PTL, until the number and size of the suspended aggregates are so large that incident light is almost totally scattered, thus drastically de-

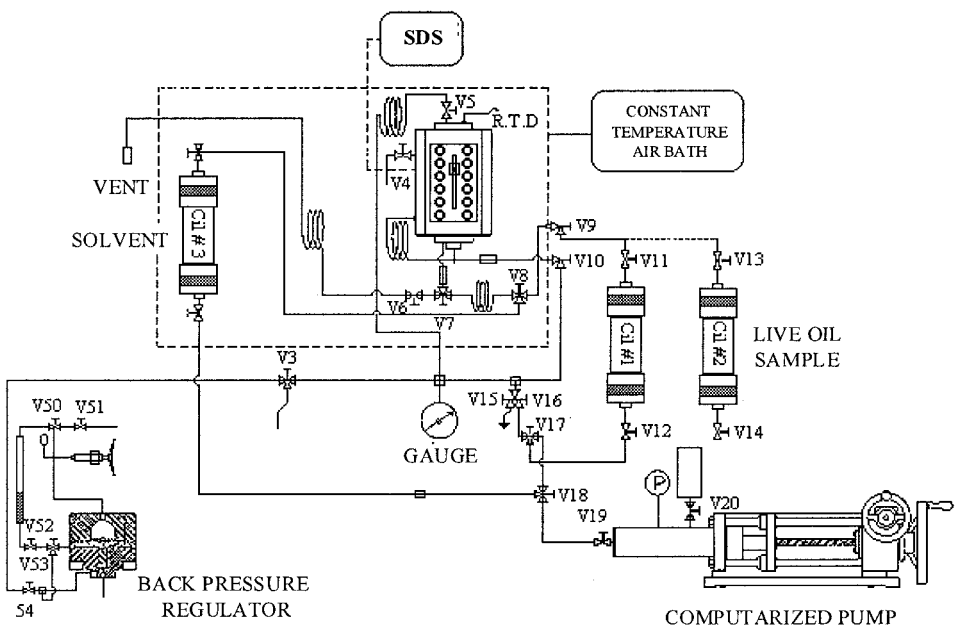

Figure 2. PVT cell with a solid detection system.

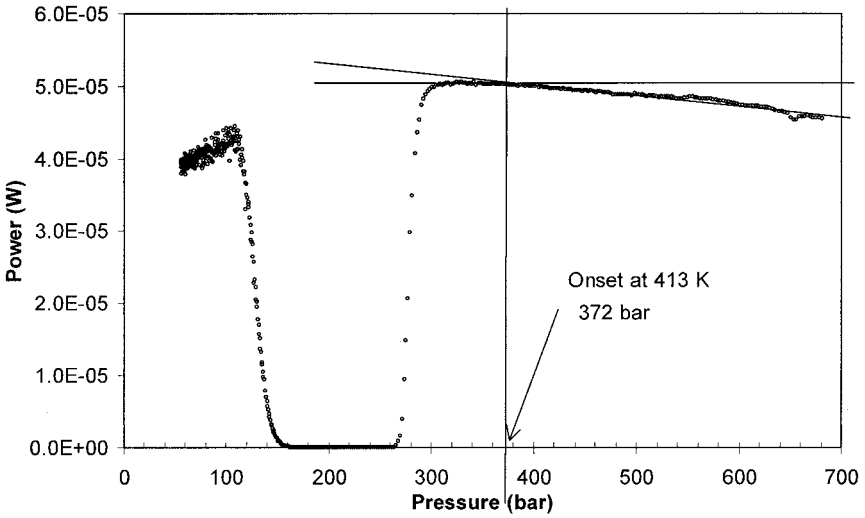

Figure 3. PTL vs. pressure plot for Y3 live oil at 413 K.

creasing the PTL. The pressure point where the PTL stops increasing continually to follow a constant tendency, or even a declining one, corresponds to the precipitation onset pressure point in a phase diagram (APE).

To illustrate how the onset points of asphaltene precipitation were determined using the SDS, Figure 3 presents the PTL vs. pressure curve for an isothermal expansion experiment of the Y3 live oil at 413 K. From the figure, it is clear that by decreasing pressure, the light transmittance increased almost linearly with the pressure, resulting from the oil expansion, but when the onset pressure is reached, asphaltene aggregates start to increase in both size and number. Under these conditions a competition begins between the increases of PTL (attributed to oil expansion) and the scatter of the incident light attributed to aggregation. Then, the increment of PTL signal stops maintaining a constant value within a certain pressure range, until the size and number of particles per volume unit of fluid are so large that they completely scatter the incident light and the PTL signal decreases dramatically to the noise level. The exact determination of the onset pressure in the curve PTL vs. pressure depends on the compressibility of the fluid and the kinetics of the aggregation. The larger the compressibility, the greater the slope of the relation between transmitted light and pressure; on the other hand, the faster the kinetics, the shorter the signal plateau, where the PTL is constant. These are the ideal conditions for an accurate onset determination. However, in our case, both oils were somewhat far from these conditions. In the case of oil Y3, the linear segment is more or less well defined, but the plateau is long and it has an up-and-down behavior. Consequently, the onset determination is highly uncertain. To avoid speculative interpretations of the PTL vs. pressure curve, a single criterion was applied in the determination of the onset pressure in all the experiments of both oils. The onset was set at the intersection of a zero-slope line drawn on the plateau of the plot, where the PTL is constant, and the straight line that best adjusted to the section of the curve where the PTL increases continuously with the decrease of pressure.

For other oils, one may encounter PTL vs. pressure curves that differ, sometimes significantly, from the behavior described before, showing nonlinear plots or positive slopes (Aquino-Olivos et al., 2001) as well. Such behavior could be attributable to a slow growth of particles or changes in the number of particles per unit volume. The nature of the oil and asphaltenes may indeed affect the trace recorded, given that sticking to the high-pressure cell windows may substantially affect the signal. Hirschberg et al. (1984) and other investigators reported how asphaltenes are observed to nucleate at the cell windows. Another possibility is that the adsorption from solution of the dissolved asphaltenes on the windows is increased even though a critical scattering size is not achieved. Finally, the possibility of breaking high-pressure emulsions by coalescence of smaller droplets may be a cause of light scattering, which has nothing to do with the formation of asphaltene particles.

When the precipitation onset pressure is reached, the isothermal expansion continues to find the highest pressure at which a bubble of gas is first liberated from the oil, that is, at the bubble point. From the pressure vs. displaced-volume plot, it is possible to infer the bubble point pressure because when the first bubble is liberated, a discontinuity occurs. This point can be found in the intersection of two lines, that is, the linear projection of the pressure–volume points at the extremes of highest pressure in the one-phase region and the lowest pressure in the liquid–vapor region, as shown in Figure 4 for the Y3 live-oil fluid at 413 K [negative values in displaced volume means the pump piston moves in backward (negative) direction during expansion]. The bubble point pressures determined in this way for the live-oil samples at the same temperatures considered for the onset-pressure determinations are reported in Table 5.

Thermodynamic Modeling

Colloidal thermodynamic theory

The phenomenon of asphaltene precipitation is a very complex multicomponent process that involves a great diversity of interactions, at molecular and colloidal length scales. Consequently, the theoretical modeling for this system is possible only by assuming simplified representations of crude oil.

A basic approximation used in solution theories is to consider the solvent as a structureless continuum with a screening

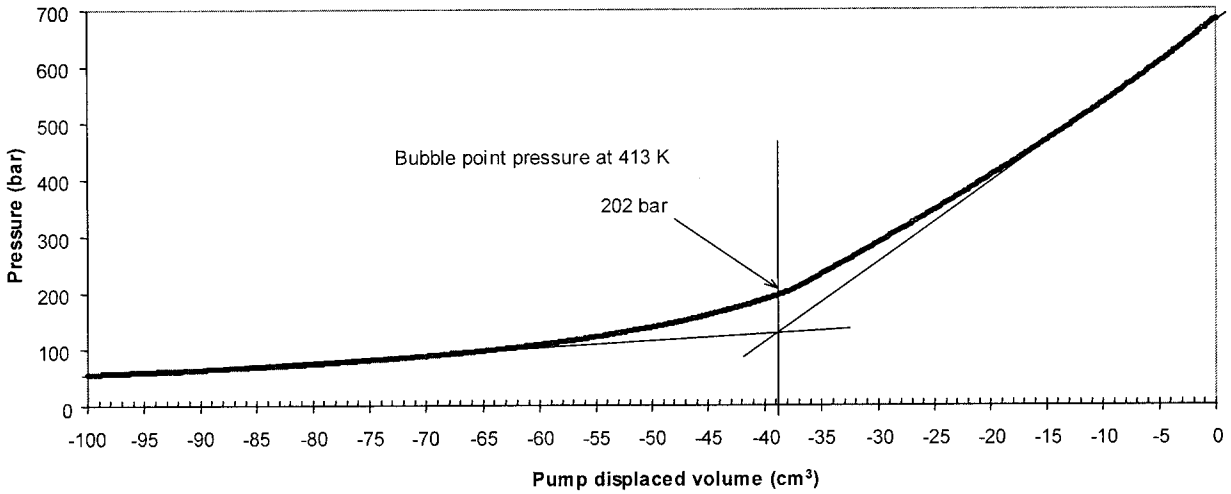

Figure 4. Pressure vs. displaced volume plot for Y3 live oil at 413 K.

effect over the interactions of solutes. This approach has been successfully used, for example, in electrolyte solutions (primitive models). In this way, the solvent is described by continuous parameters, such as the dielectric constant, refractive index, and density. A rigorous theoretical treatment of this approximation is given by the McMillan–Mayer theory of solutions, which demonstrates that the statistical mechanics of solutions can be represented through the theory of mixtures without a solvent *if and only if* the intermolecular potential between solutes is replaced by the corresponding potential of mean force (Lee, 1988; McQuarrie, 1976). Based on this approach, Wu et al. (1998) developed a simplified model to represent the asphaltene–resin–oil system by considering asphaltenes and resin as solutes dispersed in the oil (a continuous medium without structure, that is, the solvent). Details of this description are given in Wu et al. (1998, 2000). The general description can be summarized as follows: (1) asphaltene and resin are represented by pseudo-pure components, whereas all other oil components are a continuous medium; (2) asphaltene aggregates formed by several molecules are modeled as hard spheres (see Figure 5), whereas resin molecules are modeled as hard-sphere chains; (3) interactions between asphaltene and resin molecules are given by potentials of mean force and consist of hard-sphere repulsions, van der Waals attractions, and short-ranged anisotropic interactions; (4) the bonding is assumed in a way that asphaltene–asphaltene and asphaltene–resin associations are permitted, but association between resin molecules is not allowed; (5) asphaltene separation is described as a liquid–liquid equilibrium process. Although there has been speculation concerning crystallinity of the precipitated phase (McMillan et al., 1995), there is no conclusive evidence that precipitated asphaltenes form crystals under normal conditions (Hirschberg et al., 1984). On the other hand, in phase-equilibrium experiments with enriched gas–crude oil or CO_2–crude oil systems where asphaltene flocculation takes place, the third hydrocarbon phase developed has often been identified as an asphaltene-rich, second liquid phase (see Godbole et al., 1992; Monger and Fu, 1987; Shelton and Yarborough, 1977). Because the precipitated phase primarily consists of asphaltenes, it is expected that its properties are not very different from those for a solid phase as long as it is at equilibrium.

Table 5. Experimental Bubble Point Pressures of Live-Oil Samples

T	P (bar)	
(K)	C1	Y3
413.15	185.6	202.74
393.15	170.99	196.47
363.15	163.92	
354.15		180.64
348.15	139.79	
335.15		167.89

bar = 1×10^5 Pa

Following this description, asphaltene and resin molecules consist of single or chained spheres (that is, monomers, denoted by M) of different diameter, interacting by a mean-force interaction potential, expressed as

$$u_{ij}(r) = u_{ij}^{hs}(r_{ij};\ \sigma_{ij}) - \varepsilon_{ij}\phi_{ij}(r_{ij};\ \lambda_{ij}) \qquad (1)$$

where $u_{ij}^{hs}(r_{ij};\ \sigma_{ij})$ is the hard-sphere repulsive interaction defined by a diameter σ_{ij}:

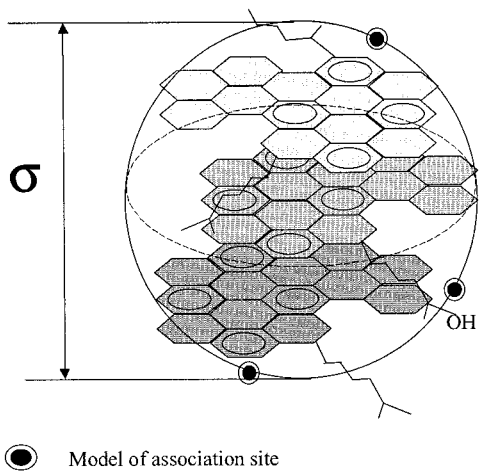

Figure 5. Detail of the asphaltene model.

Table 6. Parameters of the Thermodynamic Model

	Parameter*	Value	Determination
Monomer diameter	σ_A	1.7 nm	Experimental (Buenrostro et al., 2001b), but it can be estimated in base of Mw_A, molecular density and an estimated packing fraction.
	σ_R	0.5 nm	Estimated from density, Mw_R, molecular density and an estimated packing fraction (Wu et al., 2000)
	σ_{AR}	Calculate	From a combining rule, Eq. A19
Number of segments (monomers) in the chain	m_R	10	Estimated from density, Mw_R, molecular density and an estimated packing fraction (Wu et al., 2000)
	m_A	1	Fixed from model definitions (Wu et al., 1998)
Range of attractive potential	λ_{AA}	Adjustable	From precipitation experiments (see Table 9)
	λ_{RR}	Adjustable	From precipitation experiments (see Table 9)
	λ_{AR}	Calculated	From a combining rule, Eq. A20
Bonding volume	κ	0.05	Taken from literature (Fu and Sandler, 1995; Garcia-Lisbona, 1998; Galindo et al., 1998b; Galindo et al., 1999)
Hamaker constant	H_m	Calculated	Eq. 50 or Eq. 54
	H_A	Adjustable	From precipitation experiments (see Table 9)
	H_R	Adjustable	From precipitation experiments (see Table 9)
Association energy	ψ_{AA}	Adjustable	From precipitation experiments (see Tables 9 and 12)
	ψ_{AR}.	Adjustable	From precipitation experiments (see Tables 9 and 12)
Number of association sites	s_A	Adjustable	From precipitation experiments (see Tables 9 and 12)
	s_R	1	Fixed from model definitions (Wu et al., 1998)

*A, asphaltenes; R, resins.

$$u_{ij}^{hs}(r_{ij};\,\sigma_{ij}) = \begin{cases} \infty & r_{ij} < \sigma_{ij} \\ 0 & r_{ij} > \sigma_{ij} \end{cases} \tag{2}$$

whereas the attractive interaction has an energy depth $-\varepsilon_{ij}$ and shape $\phi_{ij}(r_{ij};\,\lambda_{ij})$, where λ_{ij} is a parameter related to the range of the attractive forces. The generic potential given by Eq. 1 depends on three parameters: σ_{ij} and ε_{ij} are the usual length and energy parameters, and λ_{ij} is the attractive potential range. By changing λ_{ij}, the shape of the attractive well is modified. To study the effect of the interaction potential model on precipitation results, we used the square well (SW) and Sutherland (S) models for ϕ_{ij}

$$\phi_{ij}^{SW}(r_{ij};\,\lambda_{ij}) = \begin{cases} 1 & \text{if } \sigma_{ij} < r_{ij} < \lambda_{ij}\sigma_{ij} \\ 0 & \text{if } r_{ij} > \lambda_{ij}\sigma_{ij} \end{cases} \tag{3}$$

and

$$\phi_{ij}^{S}(r_{ij}) = (\sigma_{ij}/r_{ij})^{\lambda_{ij}} \tag{4}$$

respectively. To estimate the energy parameter ε_{ij}, Wu et al. (1998, 2000) applied an approximation relating ε_{ij} with the Hamaker constant (Israelachvili, 1991), assuming that the medium (that is, solvent) affects the phase behavior of an asphaltene-containing crude oil only through its Hamaker constant,

$$\varepsilon_{imj} = \frac{(H_{ii}^{1/2} - H_m^{1/2})(H_{jj}^{1/2} - H_m^{1/2})}{\pi^2 \rho_i^0 \rho_j^0} \tag{5}$$

where ρ_i^0 and ρ_j^0 correspond to the number density of pure component of the species i and j, in terms of the spherical segments; H_{ii} and H_{jj} are the Hamaker constants of the species i and j; and H_m is the Hamaker constant of the medium, which depends on its properties, as explained below in the section Parameters of the Model. In Eq. 5, ε_{ij}, which corresponds to its value in vacuum (Eq. 1), has been replaced by its value in the presence of a solvent (ε_{imj}), to consider screening effects caused by the continuous medium m.

Equation of state

The general form of the Helmholtz free energy for associating chain molecules (Chapman et al., 1989, 1990) is given by

$$\frac{A}{NkT} = \frac{A^{IDEAL}}{NkT} + \frac{A^{M}}{NkT} + \frac{A^{CHAIN}}{NkT} + \frac{A^{ASSOC}}{NkT} \tag{6}$$

where A is the Helmholtz free energy for an oil of N molecules at temperature T; k is the Boltzmann constant, and A^{IDEAL}, A^{M}, A^{CHAIN}, and A^{ASSOC} are the ideal-gas, monomer, chain-formation, and association contributions to the free energy, respectively. In the SAFT-VR approach, improved expressions to represent the contributions to the free energy ascribed to dispersion and associating interactions are considered. In Appendix A the SAFT-VR expressions for the free energy contributions of Eq. 6 are given in detail.

Parameters of the Model

The parameters of our asphaltene precipitation thermodynamic model are the molecular geometry of the solutes and the strength and range of their interactions. These parameters are summarized in Table 6 and are described in this section.

Asphaltene and resin parameters

In this study, the asphaltene monomer diameter σ_A was experimentally determined by a fluorescence depolarization technique for a Mexican asphaltene, as described elsewhere (Buenrostro-Gonzalez et al., 2001b). By means of this technique, average gyration diameters from 12 to 24 Å were estimated for asphaltenes (Groenzin and Mullins, 2000). This

parameter can also be estimated from the packing fraction of the asphaltene model, given by $\eta = \pi\rho\sigma_A^3/6$, where ρ is the molecular number density and σ_A is the diameter of the hard spheres, as proposed by Wu et al. (1998).

Because resin is a liquid at ambient conditions, its packing fraction should be less than the hard-sphere solid-packing fraction at the fluid–solid phase transition (~0.55). We assume that the diameter of a resin segment is about 0.5 nm, and the number of segments per chain is about 10. With these parameters, and for a resin molecular weight $Mw_R = 800$ and mass density $d_R = 900$ kg/m^3 (Peramanu et al., 1999; Speight, 1999), the packing fraction for a pure resin chain fluid is 0.44, which is a reasonable value for high-boiling hydrocarbons.

From several studies on asphaltenes (Boduszynki, 1988; Buch et al., 2003; Groenzin and Mullins, 2000; Miller et al., 1998) there seems to be enough evidence to indicate that the average weight of an *individual* asphaltene molecule may hardly exceed 1000. However, in crude oil at ambient and high-pressure conditions, as well as in vacuum residuum and toluene solutions, asphaltenes may form aggregates of several molecules (Carnahan et al., 1993; Espinat and Ravey, 1993; Sheu and Acevedo, 2001). In our case, the molecular weight of asphaltenes measured by GPC from an asphaltene–tetrahydrofuran solution is 3066 g/mol (Buenrostro-Gonzalez et al., 2001a) (see Table 1). This corresponds to a small aggregate formed by three or four asphaltene molecular units. This aggregate is modeled as a hard sphere, as depicted in Figure 5.

Solvent parameters

The Hamaker constant of the solvent (or medium, H_m), depends on composition and density, and for asphaltene precipitation by addition of *n*-alkanes, it is calculated using a simple linear mixing rule

$$H_m = x_{oil}H_{oil} + x_{alkane}H_{alkane} \tag{7}$$

where x is the mole fraction. By assuming an oil as a liquid hydrocarbon without asphaltenes, resins and light components (CH_4, N_2, CO_2, and H_2S), and that such a liquid can be modeled as an ensemble of CH_2 groups, H_{oil} can then be estimated from the Hamaker constant definition

$$H_{oil} = \pi^2 B_{CH_2}\rho_{CH_2}^2 \tag{8}$$

Table 7. Fraction of Precipitated Material from Oil C1 (wt %)

Solvent Ratio*	nC_5	nC_7	nC_9	nC_{12}
0.52	onset	—	—	—
1	1.07	0.95	0.90	—
2	1.71	1.36	1.19	0.72
3	2.31	1.74	1.41	—
4	2.52	1.85	1.67	1.26
7	2.90	2.17	2.00	1.60
10	3.54	2.35	2.13	1.71
30	3.69	2.95	2.54	—
50	3.81	3.08	2.60	1.83

*Solvent Ratio: cm^3 of *n*-alkane per g of oil.

where $B_{CH_2} = 5 \times 10^{-78}$ J m^6 is the London dispersion constant for CH_2 groups (Israelachvili, 1991). The number density of CH_2 groups is calculated from the mass density of the oil without asphaltenes and resins, d_{oil}, as

$$\rho_{CH_2} = d_{oil}N_{AV}/W_{CH_2} \tag{9}$$

where W_{CH_2} is the CH_2 molecular weight and N_{AV} is Avogadro's number.

In the case of H_{alkane}, we use the Lifshitz formula (Israelachvili, 1991), expressed as

$$H_{alkane} = \frac{3}{4}kT\left(\frac{\varepsilon_{r\,alkane} - 1}{\varepsilon_{r\,alkane} + 1}\right)^2 + \frac{3h\nu_e}{16\sqrt{2}}\frac{(n_{alkane}^2 - 1)^2}{(n_{alkane}^2 - 1)^{3/2}} \tag{10}$$

where h is Planck's constant (6.626×10^{-34} J/s) and ν_e is the electron orbital frequency (3.3×10^{15} s^{-1}).

The calculation of asphaltene precipitation in a live-oil sample involves the estimation of the medium properties, H_m and ρ, considering the light components dissolved in oil at given values of pressure and temperature, P and T, respectively. The contribution of light components to the Hamaker constant of the medium can be estimated by a pairwise additivity approximation

$$H_m = \sum_i \sum_j \pi^2 B_{ij}\rho_i\rho_j \tag{11}$$

where $B_{ij} = \sqrt{B_iB_j}$; i and j refer to CH_4, N_2, CO_2, H_2S, and CH_2 groups; and ρ_i is the number density for each component in the liquid phase at T and P conditions. The London constants for the gases dissolved in the oil are estimated from the polarizability and the first ionization potential (Israelachvili, 1991).

Associating parameters

The associating interaction is represented by a square-well potential model, whose energy parameter ψ is fitted to experimental precipitation data, and the SW range of the association interaction determines the bonding volume κ, whose value is chosen as the same value used for other systems, such as alcohols, refrigerants, and electrolytes (Fu and Sandler, 1995; Galindo et al., 1998b, 1999; Garcia-Lisbona, 1998).

It is worth noting that all the molecular parameters required by the model (see Table 6) have a clear physical meaning based on colloidal and molecular models used to represent asphaltenes, resins, the oil, and the interactions among them. Consequently, they are not arbitrary numerical parameters. Most of the model parameters can be obtained by experimental proce-

Table 8. Fraction of Precipitated Material from Oil Y3 (wt %)

Solvent Ratio*	nC_5	nC_7	nC_9	nC_{12}
0.5	0.87	0.70	0.55	0.45
2	1.89	1.82	1.35	1.14
4	2.72	2.29	2.06	1.87
10	3.00	2.38	2.19	1.97
50	3.25	2.71	2.30	2.12

*Solvent Ratio: cm^3 of *n*-alkane per g of oil.

Table 9. Model Parameters Fitted Using Sutherland and SW Potential Models for Tank-Oil C1*

	s_A	H_A/k (K)	H_R/k (K)	λ_{AA}	λ_{RR}	ψ_{AA}/k (K)	ψ_{AR}/k (K)
Sutherland	3	11270.01	1891.03	4.130	4.200	2036.54	2383.34
SW	3	11270.01	1891.03	1.596	1.564	2036.54	2383.34

*$k = 1.381 \times 10^{-23}$ J/K (Boltzman constant). $\lambda_{ij} = (\lambda_i\sigma_i + \lambda_j\sigma_j)/(\sigma_i + \sigma_j)$.

dures, fixed by model assumptions, or calculated through specific physical relationships or recent theoretical results (Ortega-Rodriguez et al., 2004). Only seven parameters (H_A, H_R, λ_{AA}, λ_{RR}, ψ_{AA}, ψ_{AR}, and s_A) need to be determined from experimental data of the particular oil of interest.

Asphaltene Precipitation as a Liquid-Liquid Separation

The conditions for liquid–liquid isothermal equilibrium are obtained by imposing the equality of intensive thermodynamic functions in both phases:

$$\mu'_A = \mu''_A \tag{12}$$

$$\mu'_R = \mu''_R \tag{13}$$

$$\pi' = \pi'' \tag{14}$$

where superscripts $'$ and $''$ refer to the two equilibrated phases (the higher-density liquid phase corresponds to the precipitated phase); μ is the chemical potential; A and R denote asphaltenes and resins, respectively; and π denotes the osmotic pressure, recalling that, according to the McMillan–Mayer theory, the pressure to be considered must be the osmotic pressure, where only the solutes are involved in an explicit way in the thermodynamic expressions. As in the case of electrolyte solutions, the chemical potentials of the solutes and the osmotic pressure for each phase in the asphaltene–resin–oil mixture depend only on the solutes concentration (asphaltene and resin) in the solvent (oil). The osmotic pressure is obtained from the thermodynamic relationship

$$\frac{\pi V}{\hat{N}kT} = \sum_{i=1}^{2} \hat{x}_i \frac{\mu_i}{kT} - \frac{A}{\hat{N}kT} \tag{15}$$

where the chemical potential is calculated from the free energy A

$$\mu_i = \left(\frac{\partial A}{\partial N_i}\right)_{T,V,N_{j\neq i}} \qquad i = A, R \tag{16}$$

where V is the total volume of the phase. The thermodynamic properties are written in terms of effective values of composition and density, $\hat{x}_i$ and ρ, respectively, which depend only on the solutes properties,

$$\hat{N} = N_A + N_R \tag{17}$$

$$\hat{x}_i = N_i/\hat{N} \qquad i = A, R \tag{18}$$

$$\hat{\rho} = \rho_A + \rho_R \tag{19}$$

The total values for the molar fractions and densities are given by

$$x_i = \frac{N_i}{N_A + N_R + N_m} \tag{20}$$

$$\rho_i = x_i/v \qquad i = A, R \tag{21}$$

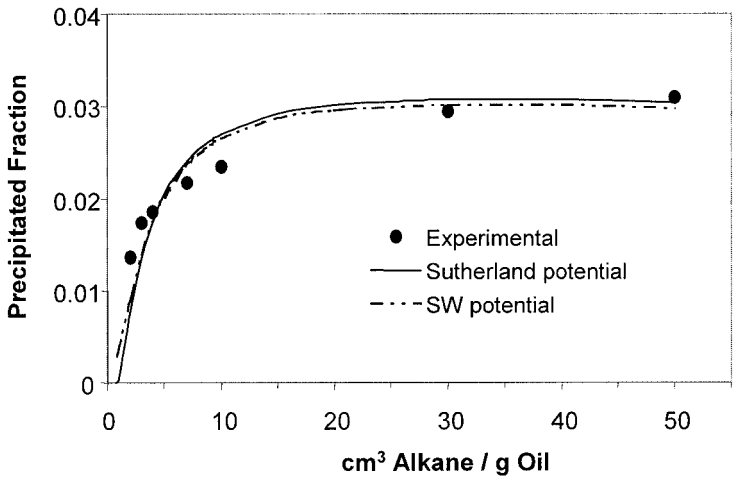

Figure 6. Fitting of experimental *n*-heptane titration data using Sutherland and SW potential models.

Table 10. Effect of the Carbon Number of Diluent on Precipitation

	nC_5	nC_7	nC_9	nC_{12}	Oil
H_m/k (K)	2865.9	3311.6	3577.2	3831.0	4692.9
ε_{AmA}/k (K)	289.5	251.5	229.9	212.8	158.5
Precipitated material (wt %)	3.81	3.08	2.60	1.83	0

where N_m is the number of molecules associated with the medium m (that is, the solvent), and v is the molar volume of the phase. From Eqs. 19 to 21, we obtain the effective molar fractions of a pseudo-binary mixture in terms of the corresponding values from the whole system

$$\widehat{x}_i = \frac{\rho_i}{\widehat{\rho}} \qquad i = A, R \tag{22}$$

where ρ_i is calculated according to Eq. 21 using the molar volume of the mixture. Because solutes and solvent are hydrocarbons, dispersion forces are the dominant interactions between components. We can then assume that the mixing volume can be neglected, that is, the molar volume for a pure component v_i^0 is very close to the partial molar volume of the component in the mixture $\bar{v}_i$, and then the molar volume of the mixture is given approximately as

$$v \approx x_A v_A^0 + x_R v_R^0 + x_m v_m^0 \tag{23}$$

To determine the coexistence values $\{N'_A, N'_R, N'_M, N''_A, N''_R, N''_M\}$ of two phases in equilibrium, where N'_i and N''_i are the molecules of species i on each phase, the equilibrium Eqs. 12–14 must be supplemented with another three equations given by the mass balance restrictions,

$$N'_i + N''_i = N_i^0 \qquad i = A, R, m \tag{24}$$

where N_i^0 is the total number of molecules of species i. The solution for the amount of precipitated material obtained through Eqs. 12–14 and 24, involves the solution of six nonlinear equations with six unknowns, giving as input the temperature T and N_i^0 ($i = A, R, m$).

In this work, the onset of asphaltene precipitation pressure is obtained through the Gibbs free energy surface analysis by minimization of the tangent plane distance (TPD) (Michelsen, 1982; Firoozabadi, 1999), expressed as

$$TPD(\boldsymbol{x}) = \sum_{i=1}^{n} x_i[\mu_i(\boldsymbol{x}) - \mu_i(\boldsymbol{z})] \tag{25}$$

where $TPD(\boldsymbol{x})$ is the tangent plane distance function evaluated at the trial second-phase composition $\boldsymbol{x}$, overall composition of the mixture $\boldsymbol{z}$, temperature, and pressure. The n value is taken as 3. Given that in the phase-stability analysis the medium must be considered together with asphaltenes and resins, the calculation of the chemical potential of the medium is described in Appendix B. When asphaltene precipitation occurs, $TPD(\boldsymbol{x}) < 0$, the amount precipitated is calculated by solving the six nonlinear equations (Eqs. 12–14 and 24) with the Broyden algorithm (Press et al., 1992), using the $\boldsymbol{x}$ values provided by phase-stability analysis as initial guesses.

Results and Discussion

Asphaltene precipitation by adding normal alkanes

In Tables 7 and 8 the weight percentage values of asphaltene precipitated, using different alkanes (nC_5, nC_7, nC_9, and nC_{12}) at ambient conditions, are given. For a given dilution ratio, the amount of asphaltenes precipitated decreases as the carbon number of the n-alkane diluent increases. The precipitation increases substantially as the solvent/oil ratio also increases, for concentrations < 10 cm^3 of n-alkane/g of oil. Beyond this value, precipitation increases by very small amounts. These general trends are similar to those observed by other investigators in similar experiments (Chung et al., 1991; Hirschberg et al., 1984; Kokal et al., 1992; Rassamdana and Sahimi, 1996). Data in the region below a ratio of 10 cm^3/g are not very

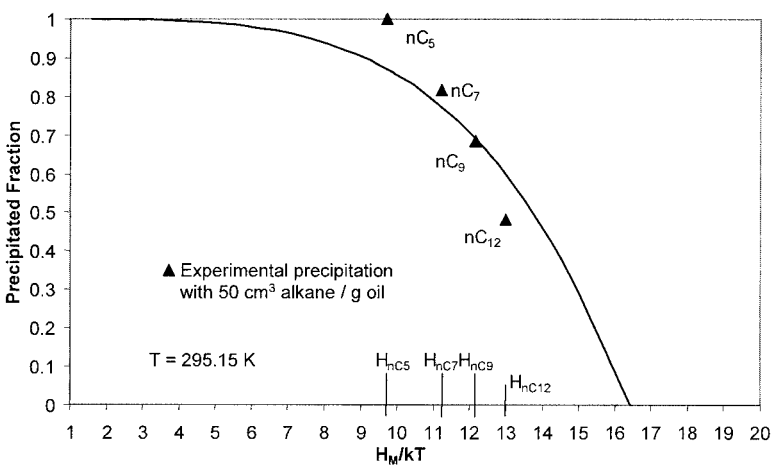

Figure 7. Effect of medium properties on asphaltene precipitation (carbon number of the precipitant).

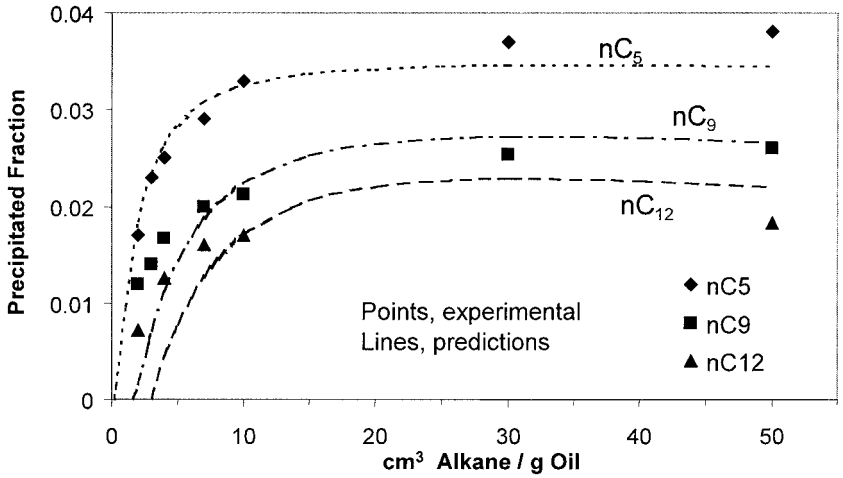

Figure 8. Prediction of asphaltene precipitation with *n*-alkanes for C1 tank oil sample.

accurate because of the viscosity of the oil–solvent solutions. However, accuracy improves at the higher solvent ratios.

Comparison between Sutherland and SW potentials

The model parameters were fitted from the *n*-heptane titration data of oil C1, for the Sutherland and SW potentials. The corresponding fitted parameters are given in Table 9. In Figure 6, the *n*-heptane titration curves for the C1 crude oil, calculated using both interaction potential models, are compared with the experimental data. In both cases, the calculated fractional precipitation is within the 13% error of the experimental value. According to these results, the use of any of these interaction potential models does not represent any appreciable difference in the representation of asphaltene precipitation. This result is explained by the fact that the association contribution to the total free energy dominates over the mean-attractive energy contribution. Thus, the model results that are presented were obtained using the Sutherland potential.

Modeling the effect of the medium properties

In titration experiments, the change of the medium or solvent properties is attributed to the dilution of the oil with a diluent (that is, the *n*-alkane). As the carbon number of the normal alkane increases, its density and dielectric constant increase as well (see Table 2). Considering a precipitant-to-oil ratio of 50 mL/g, Table 10 shows that the Hamaker constant of the medium increases as the carbon number of the precipitant increases, and that the screening effect over interactions of solutes becomes stronger, decreasing the energy parameter of the attractive potential (ε_{AmA}) and the amount of precipitated material, according to experimental results (see Figure 7). The solvent properties directly affect the mean-attractive energy term in the monomer contribution to the total Helmholtz free energy a_1. In our SAFT-VR EOS approach, the association free energy contribution also depends on a_1; then the conditions that determine the amount of precipitated material are also modified.

Prediction of asphaltene precipitation with n-alkanes

The *n*-pentane, *n*-octane, and *n*-dodecane titration curves for the crude oil C1 predicted with SAFT-VR, using the Sutherland interaction potential and the parameters fitted from the *n*-heptane titration curve alone (Table 9), are compared with the experimental data. The predicted fractional precipitation agrees well with the experimental values for the *n*-pentane titration curve only at low

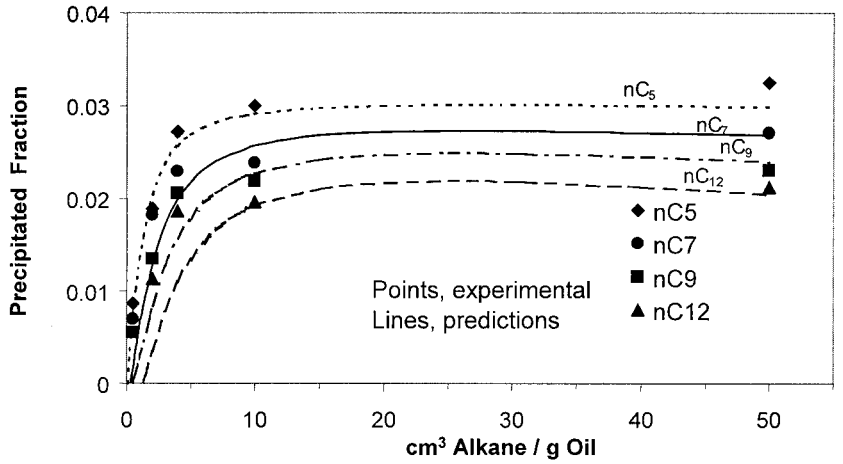

Figure 9. Prediction of the asphaltene precipitation with *n*-alkanes for Y3 tank oil sample.

Table 11. Experimental Onset Pressures of Live-Oil Samples

T	P (bar)	
(K)	C1	Y3
413.15	345.10	372.18
393.15	360.45	455.56
363.15	379.85	
354.15		474.63
348.15	386.02	
335.15		600.19

bar = 1×10^5 Pa

dilution. For *n*-nonane and *n*-dodecane the prediction is much better for high-dilution ratios than for low-dilution ratios. In all cases the predicted fractional precipitation at dilution ratios > 5 mL/g are within the 10% error of the experimental values. Figure 8 shows these comparisons in detail.

To test the predictive power of our thermodynamic model in a *different* crude oil, the prediction of a different set of experimental titration data from the Y3 stock-tank oil was studied. The predicted titration curves for the Y3 tank oil are given in Figure 9. The values of the model parameters in this case were the same fitted values used for oil C1, except for the association energy parameters ψ_{AA} and ψ_{AR}, whose values were obtained from titration data of oil Y3 with *n*-heptane. Values of the new parameters are $\psi_{AA}/k = 2062.21$ K and $\psi_{AR}/k = 2359.43$ K. No other assumptions or parameter modifications were used.

The predicted precipitation curves for oil Y3 resulted within 10% error of the experimental data for precipitant/oil ratios ≥ 10. However, for lower ratios, there are larger deviations from the experimental values, even though the model reproduces the decrease of the precipitation as the carbon number of the precipitant increases. As mentioned earlier, for the prediction of the precipitation in oil Y3, it was not necessary to refit the parameters related to the mean-attractive energy (the Hamaker constants and the range of the mean-force potentials). These results can be explained in terms of the similar properties and composition of C1 and Y3 crude oils and the use of the same values for the asphaltene and resin properties (Table 1), considering that both oils are produced in the same geographical location. However, it is more likely to be a consequence of the fact that the asphaltene precipitation upon mixing crude with normal alkanes is controlled mainly by associating interactions. Then, the parameters of the attractive mean-force potential have a secondary role in the modeling of the precipitation, although it is important to stress that in the SAFT-VR EOS approach the associating and mean-attractive energies are actually coupled by the perturbation approximation followed for the calculation of the radial distribution function at the contact value (see Appendix A).

Asphaltene precipitation at high pressure

Table 11 shows the onset pressure points of asphaltene precipitation measured at four different temperatures for the live oils C1 and Y3. These points belong to the upper boundary of the APE. It is observed that as the temperature increases, the pressure at the onset point diminishes, reflecting an increment of the asphaltene solubility with temperature. The increased solubility means that the onset of asphaltene precipitation requires a greater perturbation of the solvent or medium conditions, such as the oil density, which implies greater pressure depletion with respect to the reservoir condition.

To model asphaltene precipitation in a reservoir fluid at certain T and P conditions, the vapor–liquid equilibrium calculation of the reservoir fluid is first performed using a cubic equation of state, to obtain the composition and fluid properties of the liquid phase at equilibrium. Then, using the asphaltene–resin–oil model system described before, the phase-stability analysis is applied to find out the onset of asphaltene precipitation. When asphaltene precipitation appears, the amount of precipitated material is calculated by solving the liquid–liquid equilibrium equations.

Calculation of Medium Properties. Following Wu et al. (2000), the volume-shifted Peng–Robinson EOS (Peneloux et al., 1982; Peng and Robinson, 1976) was used to model the vapor–liquid–equilibrium to obtain the density and composition of the liquid phase. Recommended values for the binary

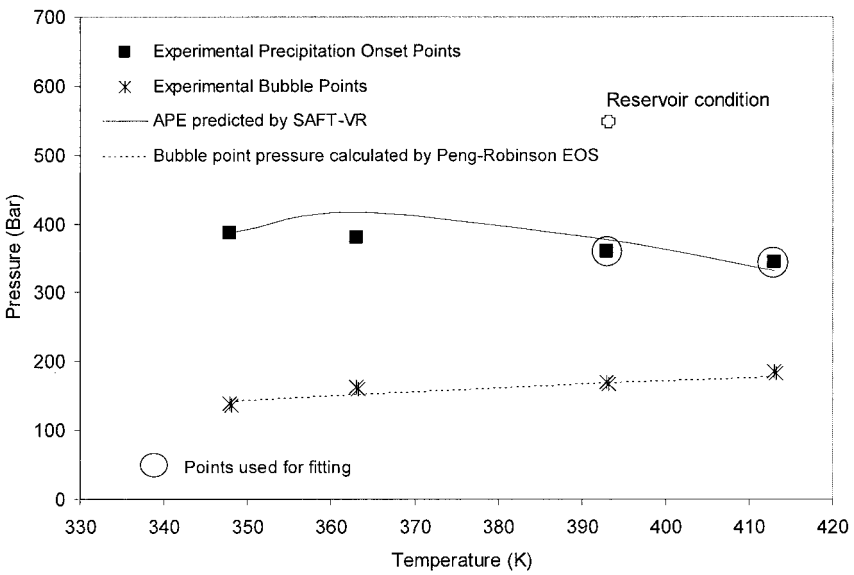

Figure 10. Comparison between experimental and predicted APE for live oil C1.

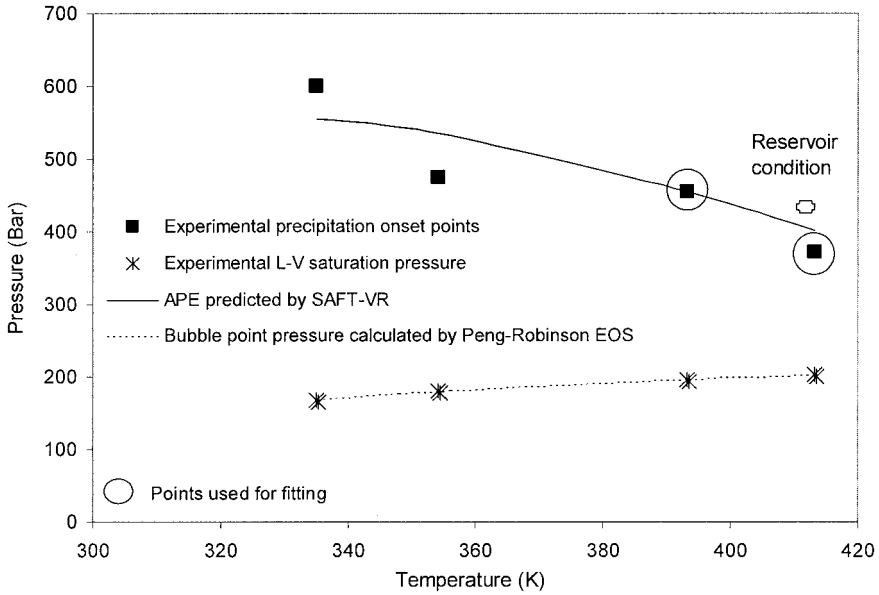

Figure 11. Comparison between experimental and predicted APE for live oil Y3.

parameters k_{ij} were used for interactions among the dissolved gases (N_2, CO_2, H_2S) and hydrocarbons (Katz and Firoozabadi, 1978). The binary interaction parameters among the hydrocarbon components are calculated according to the formula suggested by Chueh and Prausnitz (1967)

$$k_{ij} = 1 - \left[\frac{2Vc_i^{1/6}Vc_j^{1/6}}{Vc_i^{1/3} + Vc_j^{1/3}}\right]^{\theta} \tag{26}$$

where Vc is the critical volume and θ is an adjustable parameter.

The values of θ (Eq. 26) for each live oil ($\theta_{\text{live oil C1}} = 1.4$ and $\theta_{\text{live oil Y3}} = 1.65$) were obtained by matching the bubble point pressure at 393 K for oil C1 and 413 K for oil Y3. Once the composition and density of the oil, at given T and P conditions, are known, the Hamaker constant is then calculated by Eqs. 5 and 11.

Calculation of the APE. The onset points of the upper boundary of the APE for the live oils C1 and Y3 calculated by the SAFT-VR EOS, together with the bubble point line calculated by the volume-shifted Peng–Robinson EOS, are compared with the corresponding experimental data in Figures 10 and 11, respectively. The APE curves were obtained using the *same* model parameters fitted for the *n*-heptane titration data of the corresponding tank-oil sample (Table 9), except for the parameters corresponding to SAFT-VR association contribution: s_A, ψ_{AA}, and ψ_{AR}. These parameters were determined by using two APE experimental points, at 413 and 393 K, for both live oils. The parameters obtained are given in Table 12 and the calculated onset pressures are given in Table 13. The average deviations of calculated onsets with respect to the experimental data are less than 7% error for both live oils. In the case of live oil C1, the model predicts a decrease in the onset pressure at temperatures < 370 K. These results indicate that the SAFT-VR EOS used in the framework of McMillan–Mayer theory provides reasonable predictions in live-oil systems. Moreover, considering that the precipitation mechanisms in titration experiments differ substantially from those by pressure depletion, it is particularly rewarding to notice that both types of precipitation scenarios in *the same crude oils* can reasonably be predicted by the same EOS when most of the model parameters remain unchanged.

During the reservoir fluid expansion at constant temperature, the solubility of the asphaltenes is controlled by the screening effect of the medium. From Table 14 it is seen how the change of medium properties during pressure depletion modifies the values of Hamaker constant of the medium (H_m), the attractive mean-force potential strength between asphaltenes (ε_{AmA}), and also the calculated amount of precipitated material. Above the bubble point, the drop in pressure reduces the density of the reservoir fluid, which is reflected in a decrement of H_m and an increment of ε_{AmA}, after which asphaltene precipitation increases. At the bubble point (202.6 bar, at 413 K), the precipitation has a maximum value

Table 12. Association Parameters Used for APE Prediction in Live Oils

Live Oil	s_A	ψ_{AA}/k (K)	ψ_{AR}/k (K)
C1	2	1685.13	2468.68
Y3	2	1339.96	2476.63

Table 13. Calculated Onset Pressures for Live-Oil Samples Using SAFT-VR EOS

T	P (bar)	
(K)	C1	Y3
413.15	331.61	401.16
393.15	377.18	455.00
363.15	416.90	
354.15		534.89
348.15	386.00	
335.15		555.33
Avg. Dev. %*	6.22	6.24

bar = 1×10^5 Pa

*Deviation with respect to experimental values.

Table 14. Effect of the Medium Density and Vapor-Phase Formation on Asphaltene Precipitation during Isothermal Expansion of Live Oil Y3 at 413 K

P (bar)	Vapor Fraction	Medium Density (kg/m^3)	H_M/k (K)	ε_{AmA}/k (K)	Precipitated Fraction
400	0.000	632.0	1406.1	408.9	0
380	0.000	629.0	1391.0	411.3	0.00043
340	0.000	622.0	1359.0	416.6	0.00132
300	0.000	614.0	1323.9	422.3	0.00152
260	0.000	605.0	1285.4	428.7	0.00369
220	0.000	595.0	1242.4	436.1	0.00592
202.6	0.000	590.0	1222.1	439.7	0.00700
180	0.022	600.0	1326.8	421.8	0.00138
160	0.041	611.0	1437.3	403.9	0.00026
140	0.058	621.0	1565.9	384.6	0

because the medium density has a minimum. Below the bubble point, H_m is modified mainly by the change in the composition because the liquid phase has lost light components, thus increasing its density, and the screening effect over the asphaltene interactions. In consequence, ε_{AmA} decreases and the model predicts a reduction in the precipitation.

According to the model results, asphaltene–resin precipitation is dominated by interparticle forces (represented here as associative type interactions), in addition to dispersion forces. However, in colloidal systems the screening of the attractive interactions attributed to a solvent plays a very important role because they directly take into account the effect of the changes in medium conditions, particularly during pressure depletion. In the primitive-type model proposed by Wu et al. (1998, 2000) the solvent has important screening effects on the asphaltene–resin interactions, which are taken into account trough the Hamaker constant approach used for the attractive energy parameter (Eq. 5). Taking advantage of the mean-attractive energy term given by our SAFT-VR EOS approach (also used for the calculation of the chain and association free energy contributions), it is possible to model the screening effects of the medium, which reduces the effort of data regression. For the cases studied in this work, four of the seven adjustable parameters (that is, those related to the mean-force attractive potential, H_A, H_R, λ_{AA}, λ_{RR}), were fitted from the titration data of tank-oil samples using only the *n*-heptane titration results as input information. With these values, it was possible to describe asphaltene precipitation phenomena with either new *n*-alkane titrants, and in a different oil system.

As described before, the parameters of the fluid model and the SAFT-VR EOS for the asphaltene–resin–oil system are not arbitrary numerical parameters. Some of these parameters were obtained from results of precipitation experiments. Moreover, from Table 15 one can see that the values of these fitted parameters, such as the attractive mean-force potential energy parameter and the association energy, are close to values reported in the literature for intermolecular interactions such as van der Waals and hydrogen-bonding interactions, which have been recognized as part of the forces acting in molecular aggregates of asphaltenes and resins (see Israelachvili, 1991; Murgich, 2002; Ortega-Rodriguez et al., 2003; Prausnitz et al., 2000).

Conclusions

Experimental data were obtained to study the effects of temperature (up to 413 K), pressure (up to 600 bar), and composition (*n*-alkane titrations ranging from 5 to 12 carbon atoms) on asphaltene precipitation for the tank-oil and live-oil samples of the same crude oils. APE curves at high temperatures and pressures were measured for the same oil fluids. The measured data cover a broad range of conditions where different precipitation mechanisms are involved. This situation complicates any effort to represent and predict the precipitation of asphaltenic material from both processes, using a single model and a single set of parameters.

By developing a SAFT-VR EOS description of these fluids, we have shown that an improved prediction of asphaltene

Table 15. Comparison between Fitted Values for the Interaction Model Parameters and Values of Similar Interactions Taken from Literature

	Attractive Interactions		
	ε_{AmA}* (kJ/mol) This Work	ε_{AmA}** (kJ/mol) Ortega-Rodriguez et al. (2003)	Strength of typical van der Waals "bond" (kJ/mol) Israelachvili (1991)
In tank oil (oil with out titrant)	1.318	3.438	~1.0
In live oil (at bubble point)	3.559		
	Associative Interactions		
	ψ_{AA} (kJ/mol) This Work	ψ_{AR} (kJ/mol) This Work	Strength of Most H Bonds (kJ/mol) Israelachvili (1991); Prausnitz et al. (2000)
Live oil Y3 (Table 13)	11.140	20.590	10–40

*From Eq. 5 in Tables 8 and 14, multiplying ε_{AmA}/k by k and Avogadro's number.
**Mean-force potential of two asphaltene molecules in toluene by molecular mechanics and molecular dynamics simulations.

precipitation can be achieved with the use of a single set of model parameters. Our proposed method is able to capture the fundamental features of the phase separation in the asphaltene–resin–oil systems. This approach resulted in a promising modeling approach to predict the phase equilibria of asphaltene precipitation attributed to composition changes at ambient P–T conditions (that is, from tank-oil samples), as well as for pressure depletion at reservoir conditions in live-oil samples.

Notation

a = monomer free energy per segment
a_1 = first perturbation associated to the attractive energy
a_2 = second perturbation associated to the attractive energy
A = Helmholtz free energy, J
B = London dispersion constant, J/m^6
d = mass density, g/cm^3
$f_{a,b}$ = Mayer function of the a–b site–site bonding interaction
g = radial distribution function
g_1 = first perturbation associated to the radial distribution function
H = Hamaker constant, J/m^6
h = Planck's constant, J/s
k = Boltzmann's constant, J/K
$k_{i,j}$ = binary interaction parameter
$K_{a,b,i,j}$ = volume available for bonding
m = number of segments in the chain molecular model
Mw = molecular weight, g/mol
n = refractive index
N = number of molecules
N_{AV} = Avogadro's number
P = pressure, bar
P_c = critical pressure, bar
T = temperature, K
T_c = critical temperature, K
T_b = normal boiling temperature, K
TDP = tangent plane distant
r_{ij} = distance between spherical segments i and j
s = number of association sites per spherical segment
u_{ij} = interaction potential energy between i and j
v = molar volume
v_e = electron orbital frequency, 1/s
V = total volume, m^3
Vc = critical volume, m^3
x = mole fraction of one component
$\boldsymbol{x}$ = mole fractions vector
X_a = fraction of molecules not bended at site a
y_{ij} = background pair correlation function
$\boldsymbol{z}$ = mole fractions vector of the mixture before phase separation
Z_c = critical compressibility factor

Greek letters

γ = activity coefficient
$\Delta_{a,b}$ = strength of the a–b site–site bonding interaction
ε_r = dielectric constant
ε_{ij} = energy parameter of the interaction potential between i and j, J
ζ = reduced densities
ς = packing fraction
θ = Chueh–Prausnitz adjustable parameter
κ = bonding volume parameter
λ_{ij} = range of the attractive potential between i and j
$\bar{E}$ = thermal de Broglie wavelength
μ = chemical potential
π = osmotic pressure
ρ_i = molecular number density of i, 1/m^3
σ = hard-sphere diameter, Å
ϕ_{ij} = shape of the attractive potential between i and j
ψ = association energy per association site, J
ω = acentric factor

Subscripts

a, b = indexes for associations sites
A = asphaltenes
ij = cross parameter
m = medium or solvent
R = resins
s = spherical segments

Superscripts

$'$, $''$ = denotes the two equilibrated phases
$\hat{}$ = denotes the effective properties that consider only the solutes
$ASSOC$ = association contribution
$CHAIN$ = chain contribution
eff = effective property
hs = hard sphere
$IDEAL$ = ideal contribution
M = monomer or monomer contribution
osm = osmotic
SW = square well potential
S = Sutherland potential
x = mixture value pure component

Acknowledgments

This work was supported by the Molecular Engineering Research Branch of the Mexican Institute of Petroleum (IMP) under contract FIES-98-86-I (R.00077). The authors thank PEMEX E&P for providing oil samples, and M. A. Aquino-Olivos and A. Rios-Reyes, both from the IMP, for excellent laboratory assistance. Professor J. Murgich (Instituto Venezolano de Investigacion Cientifica) is also thanked for various fruitful discussions.

Literature Cited

Andersen, S. I., "Dissolution of Solid Boscan Asphaltenes in Mixed Solvents," *Fuel Sci. Technol. Int.*, **12**, 51 (1994).
Aquino-Olivos, M. A., S. I. Andersen, and C. Lira-Galeana, "Comparisons Between Asphaltenes from the Dead and Live-Oil Samples of the Same Crude Oils," *Petrol. Sci Technol.*, **21**, 1017 (2003).
Aquino-Olivos, M. A., E. Buenrostro-Gonzalez, S. I. Andersen, and C. Lira-Galeana, "Investigation of Inhibition of Asphaltene Precipitation at High Pressure Using Bottomhole Samples," *Energy Fuels*, **15**, 236 (2001).
Bilheimer, J. S., B. H. Sage, and W. N. Lacey, "Multicondensate Phases in the *n*-Pentane–Tetralin–Butane System," *Trans. AIME*, **Nov.**, 283 (1949).
Boduszynski, M. M., "Composition of Heavy Petroleums. 2. Molecular Characterization," *Energy Fuels*, **2**, 597 (1988).
Boublík, T. J., "Hard Sphere Equation of State," *Chem. Phys.*, **53**, 471 (1970).
Buch, L., H. Groenzin, E. Buenrostro-Gonzalez, S. I. Andersen, C. Lira-Galeana, and O. C. Mullins, "Molecular Size of Asphaltene Fractions Obtained from Residuum Hydrotreatment," *Fuel*, **82**, 1075 (2003).
Buckley J. S. "Prediction the Onset of Asphaltene Precipitation from Refractive Index Measurements," *Energy Fuels*, **13**, 328 (1999).
Buenrostro-Gonzalez, E., M. Espinosa-Peña, S. I. Andersen, and C. Lira-Galeana, "Characterization of Asphaltenes and Resins from Problematic Mexican Crude Oils," *Petrol. Sci. Technol.*, **19**, 299 (2001a).
Buenrostro-Gonzalez, E., H. Groenzin, C. Lira-Galeana, and O. C. Mullins, "The Overriding Chemical Principles that Define Asphaltenes," *Energy Fuels*, **15**, 972 (2001b).
Burke, N. E., R. E. Hobbs, and S. F. Kashou, "Measurement and Modeling of Asphaltene Precipitation," *J. Petrol Technol.*, **42**, 1440 (1990).
Carnahan, N. F., L. Quintero, D. M. Pfund, J. L. Fulton, R. D. Smith, M. Lapel, and K. Leontaritis, "A Small Angle X-ray Scattering Study of the Effect of Pressure on the Aggregation of Asphaltene Fractions in Petroleum Fluids Under Near-Critical Solvent Conditions," *Langmuir*, **9**, 2035 (1993).
Chapman, W. G., K. E. Gubbins, G. Jackson, and M. Radosz, "SAFT: Equation of State Solution Model for Associating Fluids," *Fluid Phase Equilibria*, **52**, 31 (1989).
Chapman, W. G., K. E. Gubbins, G. Jackson, and M. Radosz, "New Reference Equation of State for Associating Liquids," *Ind. Eng. Chem. Res.*, **29**, 1709 (1990).
Chueh, P. L., and J. M. Prausnitz, "Vapor–Liquid Equilibria at High

Pressures: Calculation of Partial Molar Volume in Non Polar Liquid Mixtures," *AIChE J.*, **13**, 1099 (1967).
Chung, F., P. Sarthi, and R. Jones, "Modeling of Asphaltene and Wax Precipitation," Topical Report NIPER-498, U.S. Dept. of Energy, January (1991).
Davies, L. A., A. Gil-Villegas, and G. Jackson, "An Analytical Equation of State for Chain Molecules Formed from Yukawa Segments," *J. Chem. Phys.*, **111**, 8659 (1999).
De Boer, R., K. Leeloyer, M. Eigner, and A. van Bergen, "Screening of Crude Oils for Asphalt Precipitation: Theory, Practice, and the Selection of Inhibitors," *Soc. Petrol. Eng.*, **Feb.**, 55 (1995).
Espinat, D., and J. C. Ravey, "Colloidal Structure of Asphaltene Solutions and Heavy-Oil Fractions Studied by Small Angle Neutron and X-Ray Scattering," SPE 25187, SPE International Symposium on Oilfield Chemistry, New Orleans, LA, (Mar. 2–5, 1993).
Firoozabadi, A., *Thermodynamics of Hydrocarbon Reservoirs*, McGraw-Hill, New York (1999).
Fotland, P., H. Anfinsen, H. Foerdedal, and H. P. Hjermstad, "The Phase Diagrams of Asphaltenes: Experimental Technique, Results and Modeling on Some North Sea Crude Oils," Symposium on the Chemistry of the Asphaltene and Related Substances, Cancun, Mexico (1997).
Fu, Y.-H., and S. I. Sandler, "A Simplified SAFT Equation of State for Associating Compounds and Mixtures," *Ind. Eng. Chem. Res.*, **34**, 1897 (1995).
Galindo, A., L. A. Davies, A. Gil-Villegas, and G. Jackson, "The Thermodynamics of Mixtures and the Corresponding Mixing Rules in the SAFT-VR Approach for Potentials of Variable Range," *Mol. Phys.* **93**, 241 (1998a).
Galindo, A., A. Gil-Villegas, G. Jackson, and A. N. Burgess, "SAFT-VRE: Phase Behavior of Electrolyte Solutions with the Statistical Associating Fluid Theory for Potentials of Variable Range," *J. Phys. Chem. B*, **103**, 10272 (1999).
Galindo, A., A. Gil-Villegas, P. J. Whitehead, G. Jackson, and A. N. Burgess, "Prediction of Phase Equilibria for Refrigerant Mixtures of Difluoromethane (HFC-32), 1,1,1,2-Tetrafluorethane (HFC-134a), and Pentafluoroethane (HFC-125a) using SAFT-VR," *J. Phys. Chem. B*, **102**, 7632 (1998b).
Garcia-Lisbona, N. M., A. Galindo, G. Jackson, and A. N. Burgess, "Predicting the High-Pressure Phase Equilibria of Binary Aqueous Solutions of 1-Butanol, *n*-Butoxyethanol and *n*-Decylpentaoxyethylene Ether ($C_{10}E_{10}$) using SAFT-HS Approach," *Mol. Phys*., **93**, 57 (1998).
Gil-Villegas, A., A. Galindo, P. J. Whitehead, S. Mills, and G. Jackson, "Statistical Associating Fluid Theory for Chain Molecules with Attractive Potentials of Variable Range," *J. Chem. Phys.*, **106**, 4168 (1997).
Godbole, S. P., and K. J. Thele, "EOS Modeling and Experimental Observations of Three-Hydrocarbon-Phase Equilibria," SPE 24936, SPE Annual Technical Conference and Exhibition, Washington, DC, Oct. 4–7 (1992).
Groenzin, H., and O. Mullins, "Molecular Size and Structure of Asphaltenes from Various Sources," *Energy Fuels*, **14**, 667 (2000).
Hammami, A., C. H. Phelps, T. Monger-McClure, and T. M. Little, "Asphaltene Precipitation from Live Oils; An Experimental Investigation of Onset Conditions and Reversibility," *Energy Fuels*, **14**, 14 (2000).
Hirschberg, A., L. N. J. de Jong, B. A. Schipper, and J. G. Meyers, "Influence of Temperature and Pressure on Asphaltene Flocculation," *Soc. Petrol. Eng. J.*, **June**, 283 (1984).
Islam, M. R., "Role of Asphaltenes on Oil Recovery and Mathematical Modeling," *Asphaltenes and Asphalts*, Vol. 1, T. F. Yen and G. Chilingarian, eds., Elsevier Science, Amsterdam, The Netherlands, p. 249 (1994).
Israelachvili, J. N., *Intermolecular and Surface Forces*, Academic Press, San Diego, CA (1991).
James, N. E., and A. K. Mehrotra, "V-L-S Multiphase Equilibrium in Bitmen-Diluent System," *Can. J. Chem. Eng.*, **66**, 870 (1988).
Joshi, N. B., O. C. Mullins, A. Jamaluddin, J. Creek, and J. McFadden, "Asphaltene Precipitation from Live Crude Oil," *Energy Fuels*, **15**, 979 (2001).
Katz, D. L., and A. Firoozabadi, "Predicting Phase Behavior of Condensate/Crude-Oil Systems Using Methane Interaction Coefficients," *J. Petrol. Technol.*, **Nov.**, 1649 (1978).
Kawanaka, S., S. J. Park, and G. A. Mansoori, "Organic Deposition from Reservoir Fluids: A Thermodynamic Predictive Technique," *SPE Reservoir Eng.*, **May**, 185 (1991).
Kohse, B. F., L. X. Nghiem, H. Maeda, and K. Ohno, "Modelling Phase Behavior Including the Effect of Pressure and Temperature on Asphaltene Precipitation," SPE 64465, SPE Asia Pacific Oil and Gas Conference and Exhibition, Brisbane, Australia, Oct. 16–18 (2000).
Kokal, S. L., J. Najman, S. G. Sayegh, and A. E. George, "Measurement and Correlation of Asphaltene Precipitation from Heavy Oils by Gas Injection," *J. Can. Petrol. Technol.*, **31**, 24 (1992).
Kokal, S. L., and S. G. Sayegh, "Asphaltenes: The Cholesterol of Petroleum," SPE 29787 presented at the SPE Middle East Oil Show, Bharain, Mar. 11–14 (1995).
Koots, J. A., and J. G. Speight, "Relation of Petroleum Resins to Asphaltenes," *Fuel*, **54**, 179 (1975).
Lee, L. L., *Molecular Thermodynamics of Nonideal Fluids*, Butterworths, Boston, MA (1988).
Leontaritis, K. J., "The Asphaltene and Wax Deposition Envelopes," *Fuel Sci. Technol. Int.*, **14**, 13 (1996).
Leontaritis, K. J., and G. A. Mansoori, "Asphaltene Flocculation During Oil Production and Processing: A Thermodynamic Colloidal Model," SPE 16258, SPE International Symposium on Oil Field Chemistry, San Antonio, TX, Feb. 4–6 (1987).
Leontaritis, K. J. and G.A. Mansoori, "Asphaltene Deposition. A Survey of Field Experiences an Research Approaches," *J. Petrol. Sci. Eng.*, **1**, 229 (1988).
Lhioreau, C., J. Briant, and R. Tindy, "Influence de la Pression sur la Floculation des Asphaltenes," *Rev. Inst. Fr Pét.*, **22**, 797 (1967).
Lira-Galeana, C., and A. Hammami, "Wax Precipitation in Petroleum Fluids: A Review," *Asphaltenes and Asphalts*, Vol. 2, T. F. Yen and G. Chilingar, eds., Elsevier Science, Amsterdam, Chap. 21 (2000).
MacMillan, D. J., J. E. Tackett, M. A. Jessee, and T. G. Monger-McClure, "A Unified Approach to Asphaltene Precipitation: Laboratory Measurement and Modeling," *J. Petrol. Technol.*, **47**, 788 (1995).
Mannistu, K. D., H. W. Yarranton, and J. H. Masliyah, "Solubility Modeling of Asphaltenes in Organic Solvents," *Energy Fuels*, **11**, 615 (1997).
Mansoori, G. A., N. F. Carnahan, K. E. Starling, and J. Leland, "Equilibrium Thermodynamic Properties of the Mixture of Hard Spheres," *Chem. Phys.*, **54**, 1523 (1971).
McQuarrie, D., *Statistical Mechanics*, Harper-Collins, New York (1976).
Michelsen, M. L., "The Isothermal Flash Problem," *Fluid Phase Equilibria*, **82**, 117 (1982).
Miller, J. T., R. B. Fisher, P. Thiyagarajan, R. E. Winans, and J. E. Hunt, "Subfractionation and Characterization of Mayan Asphaltene," *Energy Fuels*, **12**, 1290 (1998).
Monger, T. G., and J. C. Fu, "The Nature of CO_2 Induce Organic Deposition," SPE 16713, SPE Annual Technical Conference and Exhibition, Dallas, TX, Sep. 27–30 (1987).
Müller, E. A., and K. E. Gubbins, "Molecular-Based Equations of State for Associating Fluids: A Review of SAFT and Related Approaches," *Ind. Eng. Chem. Res.*, **40**, 2193 (2001).
Murgich, J., "Intermolecular Forces in Aggregates of Asphaltenes and Resins," *Petrol. Sci. Technol.*, **20**, 983 (2002).
Nagarajan, R., and E. Ruckenstein, "Theory of Surfactant Self-Assembly: A Predictive Molecular Thermodynamic Approach," *Langmuir*, **7**, 2934 (1991).
Ortega-Rodriguez, A., S. A. Cruz, A. Gil-Villegas, F. Guevara-Rodriguez, and C. Lira-Galeana, "Molecular View of the Asphaltene Aggregation Behavior in Asphaltene–Resin Mixtures," *Energy Fuels*, **17**, 1100 (2003).
Ortega-Rodriguez, A., Y. Duda, F. Guevara-Rodriguez, and C. Lira-Galeana, "Stability and Aggregation of Asphaltenes in Asphaltene–Resin–Solvent Mixtures," *Energy Fuels*, **18**(3), 674 (2004).
Pan, H. Q., and A. Firoozabadi, "Thermodynamic Micellization Model for Asphaltene Precipitation from Reservoir Crude at High Pressure and Temperatures," SPE 38857, SPE Annual Technical Conference and Exhibition, San Antonio, TX, Oct. 5–8 (1997).
Pan, H. Q., and A. Firoozabadi, "Complex Multiphase Equilibrium Calculations by Direct Minimization of Gibbs Free Energy Using Simulated Annealing," *SPE Res. Eval. & Eng.*, **Feb.**, 36 (1998).
Peneloux, A., E. Rauzy, and R. Freze, "A Consistent Correlation for Redlich–Kwong–Soave Volumes," *Fluid Phase Equilibria*, **8**, 7 (1982).
Peng, D. Y., and D. B. Robinson, "A New Two-Constant Equation of State," *Ind. Eng. Chem. Fundam.*, **15**, 59 (1976).
Peramanu, S., B. B. Pruden, and P. Rahimi, "Molecular Weight and Specific Gravity Distributions for Athabasca and Cold Lake Bitumens and Their Saturate, Aromatic, Resin and Asphaltene Fractions," *Ind. Eng. Chem. Res.*, **38**, 3121 (1999).
Prausnitz, J., M. R. N. Lichtenthaler, and G. G. Azevedo, *Termodinámica*

Molecular de los Equilibrios de Fases, 3rd ed., Prentice-Hall, Madrid (2000).
Press, W. H., S. A. Teukolsky, W. T. Vetterling, and B. P. Flannery, *Numerical Recipes: The Art of Scientific Computing*, 2nd Edition, Cambridge Univ. Press, New York (1992).
Rassamdana, H., and M. Sahimi, "Asphaltene Floculation and Deposition. 1. Onset of Precipitation," *AIChE J.*, **42**, 3318 (1996).
Reid, R. C., J. M. Prausnitz, and B. E. Poling, *Properties of Gases and Liquids*, 4th Edition, McGraw Hill, New York (1984).
Shelton, J. L., and L. Yarborough, "Multiple-Phase Behavior in Porous Media during CO_2 of Rich-Gas Flooding," *J. Petrol. Technol.*, **Sep.**, 1171 (1977).
Sheu, E., and S. Acevedo, "Effect of Pressure and Temperature on Colloidal Structure of Furrial Crude Oil," *Energy Fuels*, **15**, 702 (2001).
Shields, D., "Predicting Asphaltene and Wax Deposition Problems in Mexican Wells," *Offshore*, **Sep.**, 84 (2000).
Speight, J. G., *The Chemistry and Technology of Petroleum*, Marcel Dekker, New York (1999).
Thomas, F. B., D. B. Bennion, D. W. Bennion, and B. E. Hunter, "Experimental and Theoretical Studies of Solids Precipitation from Reservoir Fluid," *J. Can. Petrol. Technol.*, **31**, 22 (1992).
Ting, P. D., G. J. Jirasaki, and W. G. Chapman, "Modeling of Asphaltene Phase Behavior with the SAFT Equation of State," *Petrol. Sci. Technol.*, **21**, 647 (2003).
Tutle, R. N., "High-Pour-Point and Asphaltic Crude Oils and Condensates," *J. Petrol. Technol.*, **21**, 1192 (1983).
Twu, C. H., "An Internally Consistent Correlation for Predicting the Critical Properties and Molecular Weights of Petroleum and Coal-Tar Liquids," *Fluid Phase Equilibria*, **16**, 137 (1984).
Victorov, A. I., and A. Firoozabadi, "Thermodynamic Micellization Model of Asphaltene Precipitation from Petroleum Fluids," *AIChE J.*, **42**, 1753 (1996).
Wu, J., J. M. Prausnitz, and A. Firoozabadi, "Molecular–Thermodynamic Framework for Asphaltene–Oil Equilibria," *AIChE J.*, **44**, 1188 (1998).
Wu, J., J. M. Prausnitz, and A. Firoozabadi, "Molecular Thermodynamics of Asphaltene Precipitation in Reservoir Fluids," *AIChE J.*, **46**, 197 (2000).
Yarranton, H. W., and J. H. Masliyah, "Molar Mass Distribution and Solubility Modeling of Asphaltenes," *AIChE J.*, **42**, 3533 (1996).

Appendix A: SAFT-VR Equation of State

Ideal contribution

$$\frac{A^{Ideal}}{NkT} = \left(\sum_{i=1}^{n} x_i \ln \rho_i \Lambda_i^3 \right) - 1 \tag{A1}$$

where ρ_i is the number density of molecules (chains), x_i is the molar fraction, and $\Lambda = h/\sqrt{2\pi mkT}$ is the thermal de Broglie wavelength (h is Planck's constant and m is the molecular mass).

Monomer contribution

$$\frac{A^{Mono}}{NkT} = \left(\sum_{i=1}^{n} x_i m_i \right) \frac{A^M}{N_S kT} = \left(\sum_{i=1}^{n} x_i m_i \right) a^M \tag{A2}$$

where m_i is the number of spherical segments of chain i and N_s is the total number of spherical segments. The monomer free energy per segment a^M is obtained from a high-temperature expansion, expressed as

$$a^M = a^{hs} + \beta a_1 + \beta^2 a_2 \tag{A3}$$

where $\beta = 1/kT$; a^{hs} is the Helmholtz free energy of hard spheres; and a_1 and a_2 are the first and second perturbation terms, respectively, associated with the attractive energy. The second-order term a_2 is described in detail by Gil-Villegas et al. (1997) and Galindo et al. (1998a). In our study we found that the inclusion of a_2 did not improve the description of asphaltene precipitation; then the results discussed are restricted to the first-order perturbation theory.

The free energy a^{hs} is obtained from the Carnahan–Starling–Mansoori–Boublik expression (Boublik, 1970; Mansoori et al., 1971)

$$a^{hs} = \frac{6}{\pi \rho_s} \left[\left(\frac{\zeta_2^3}{\zeta_3^2} - \zeta_0 \right) \ln(1 - \zeta_3) + \frac{3\zeta_1 \zeta_2}{1 - \zeta_3} + \frac{3\zeta_2^3}{\zeta_3 (1 - \zeta_3)^2} \right] \tag{A4}$$

where $\rho_s = N_s/V = \rho(\sum_i^n x_i m_i)$ and ρ is the total molecular density of the mixture. The reduced densities ζ_l are defined as

$$\zeta_l = \frac{\pi}{6} \rho_s \left[\sum_{i=1}^{n} x_{s,i} (\sigma_i)^l \right] \tag{A5}$$

where σ_i is the diameter of spherical segments of chain i and $x_{s,i}$ is the fraction of segments of type i in the mixture. The overall packing fraction of the mixture is given by ζ_3.

The mean-attractive energy term a_1 is given by the sum of the corresponding attractive interaction terms a_1^{ij}

$$a_1 = \sum_{i=1}^{n} \sum_{j=1}^{n} x_{s,i} x_{s,j} a_1^{ij} \tag{A6}$$

where a_i^{ij} is expressed by

$$a_i^{ij} = -2\pi \rho_s \varepsilon_{ij} g_{ij}^{hs}(\sigma_{ij}; \zeta_x^{eff}) \int_{\sigma_{ij}}^{\infty} r_{ij}^2 \phi_{ij}(r_{ij}) dr_{ij} \tag{A7}$$

where $g_{ij}^{hs}(\sigma_{ij}; \zeta_x^{eff})$ is the contact value of the hard sphere radial distribution function evaluated at an effective packing fraction ζ_x^{eff}

$$g_{ij}^{hs}(\sigma_{ij}; \zeta_x^{eff}) = \frac{1}{1 - \zeta_x^{eff}} + 3 \frac{D_{ij} \zeta_x^{eff}}{(1 - \zeta_x^{eff})^2} + 2 \frac{(D_{ij} \zeta_x^{eff})^2}{(1 - \zeta_x^{eff})^3} \tag{A8}$$

where

$$D_{ij} = \frac{\sigma_i \sigma_j \sum_{i=1}^{n} x_{s,i} \sigma_i^2}{(\sigma_i + \sigma_j) \sum_{i=1}^{n} x_{s,i} \sigma_i^3} \tag{A9}$$

and

$$\zeta_x^{eff}(\zeta_x, \lambda_{ij}) = c_1(\lambda_{ij}) \zeta_x^1 + c_2(\lambda_{ij}) \zeta_x^2 + c_3(\lambda_{ij}) \zeta_x^3 \tag{A10}$$

The effective packing fraction in Eq. A10 is calculated from a van der Waals one-fluid packing fraction of the mixture, ζ_x

$$\zeta_x = \frac{\pi}{6}\rho_s \sum_{i=1}^{n}\sum_{j=1}^{n} x_{s,i}x_{s,j}\sigma_{ij}^3 \tag{A11}$$

and the constants c_1, c_2, and c_3 in Eq. A11 are constants dependent on the specific potential shape assumed for the attractive interactions (Gil-Villegas et al., 1997).

Chain contribution

$$\frac{A^{chain}}{NkT} = -\sum_{i=1}^{n} x_i(m_i - 1)\ln y_{ii}^M(\sigma_{ii}) \tag{A12}$$

where the background pair correlation function at contact of the monomers $y_{ii}^M(\sigma_i)$ is given by the pair radial distribution function at contact

$$y_{ij}^M(\sigma_{ij}) = g_{ij}^M(\sigma_{ij})e^{-\beta\varepsilon_{ij}} \tag{A13}$$

The pair function $g_{ii}^M(\sigma_i)$ is also calculated from a high-temperature perturbation theory

$$g_{ij}^M(\sigma_{ij}) = g_{ij}^{hs}(\sigma_{ij}) + \beta\varepsilon_{ij}g_1(\sigma_{ij}) \tag{A14}$$

The term $g_1(\sigma_{ij})$ in Eq. A14 can be calculated directly from the first-order term a_1 as it is described in Gil-Villegas et al. (1997).

Associating contribution

$$\frac{A^{assoc}}{NkT} = \sum_{i=1}^{n} x_i\left[\sum_{a=1}^{S_i}\left(\ln X_{\alpha,i} - \frac{X_{\alpha,i}}{2}\right) + \frac{s_i}{2}\right] \tag{A15}$$

Equation A15 is obtained from the perturbation theory of Wertheim for associating fluids (Chapman et al., 1990); the first sum is over the species i, and the second is over all the s_i associating sites a on the molecule of type i. The fraction $X_{a,i}$ of molecules of species i not bonded at site a is

$$X_{\alpha,i} = \frac{1}{1 + \sum_{j=1}^{n}\sum_{b=1}^{s_j}\rho x_j X_{b,j}\Delta_{a,b,i,j}} \tag{A16}$$

where

$$\Delta_{a,b,i,j} = K_{a,b,i,j}f_{a,b,i,j}g_{ij}^M(\sigma_{ij}) \tag{A17}$$

The parameter $\Delta_{a,b,i,j}$ is specific for each a–b site–site bonding interaction and incorporates the strength of the association interaction using the Mayer function (Lee, 1988)

$$f_{a,b,i,j} = \exp\left(\frac{-\psi_{a,b,i,j}}{kT}\right) - 1 \tag{A18}$$

of the SW bonding $\psi_{a,b,i,j}$ as well as the volume available for bonding $K_{a,b,i,j}$.

The cross parameters of the mixture are calculated by the combining rules (Galindo et al., 1998a), expressed by the following

$$\sigma_{ij} = \frac{\sigma_i + \sigma_j}{2} \tag{A19}$$

$$\lambda_{ij} = \frac{\lambda_i\sigma_i + \lambda_j\sigma_j}{\sigma_i + \sigma_j} \tag{A20}$$

Appendix B: Chemical Potential of the Medium

From definitions of fugacity and activity coefficient of the component m, $\gamma_m \equiv a_m/x_m$ (Prausnitz et al., 2000) we obtain the following equation

$$RT\ln(x_m\gamma_m) = \mu_m - \mu_m^0 \tag{B1}$$

which can be combined with

$$-\ln a_m = \frac{\pi v_m^0}{RT} \tag{B2}$$

to obtain the chemical potential of the medium μ_m

$$\mu_m = \mu_m^0 - \pi v_m^0 \tag{B3}$$

where v_m^0 is the molar volume of the medium as pure component; μ_m^0 is the standard chemical potential of the medium, which is independent of the composition; and π is the osmotic pressure calculated from Eq. 15.

Manuscript received Oct. 24, 2003, and revision received Feb. 24, 2004.